Journal of Medicinal Chemistry

pubs.acs.org/jmc

Article

Structural Insights into Protein-Inhibitor Interactions in Human Tryptophan Dioxygenase

Zachary Geeraerts, Izumi Ishigami, Ariel Lewis-Ballester, Khoa N. Pham, Arina Kozlova, Caroline Mathieu, Raphaël Frédérick, and Syun-Ru Yeh*

Cite This: *J. Med. Chem.* 2024, 67, 14543−14552

Read Online

ACCESS | Metrics & More | Article Recommendations | Supporting Information

ABSTRACT: Human tryptophan dioxygenase (TDO) and indoleamine 2,3-dioxygenase (IDO) are two important targets in cancer immunotherapy. Extensive research has led to a large number of potent IDO inhibitors; in addition, 52 structures of IDO in complex with inhibitors with a wide array of chemical scaffolds have been documented. In contrast, progress in the development of TDO inhibitors has been limited. Only four structures of TDO in complex with competitive inhibitors that compete with the substrate L-tryptophan for binding to the active site have been reported to date. Here we systematically evaluated the structures of TDO in complex with competitive inhibitors with three types of pharmacophores, imidazo-isoindole, indole-tetrazole, and indole-benzotriazole. The comparative assessment of the protein-inhibitor interactions sheds new light into the structure-based design of enzyme-selective inhibitors.

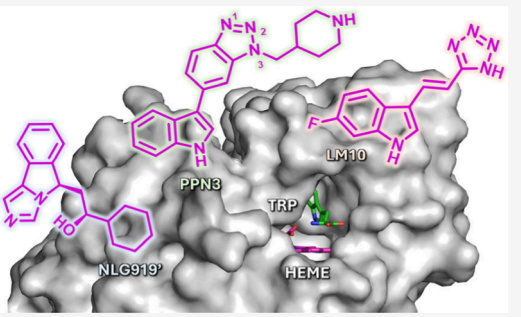

INTRODUCTION

Tryptophan dioxygenase (TDO) and indoleamine-2,3-dioxygenase (IDO) are the only two heme-based dioxygenases in humans that catalyze the first and rate-limiting step of the kynurenine pathway, the dioxygenation of L-tryptophan (Trp) to N-formyl kynurenine.[1−4] The kynurenine pathway represents the primary route for Trp metabolism, accounting for ∼95% of Trp catabolism.[5,6] The two dioxygenases hence play a vital role in controlling the systemic Trp flux. In addition to the house-keeping function, TDO and IDO are highly expressed in some cancer cells, where they function as immunosuppressors to promote cancer immune escape.[7−12] Accordingly, they have been considered as two key cancer immunotherapeutic drug targets. A great deal of research in drug discoveries targeting each enzyme have been initiated.[13−23] Although TDO and IDO were discovered in 1930s and 1960s, respectively, the three-dimensional structure of human IDO was not solved until 2006, based on two substrate-free derivatives,[24] while that of the Trp complex was not documented until a decade later.[25] The structure of human TDO, on the other hand, was first reported in 2016 based on Trp-bound complexes.[26] These structural data have been instrumental in guiding structure-based inhibitor design.

TDO is a tetramer organized as a dimer of dimers (Figure S1A). Each dimer in TDO is stabilized by domain swapping of a small N-terminal domain. Each monomer contains three domains: (i) the active site domain containing a heme prosthetic group that is coordinated by a histidine (H328), (ii) the Helix−loop−Helix domain extending out of the active site domain, and (iii) the N-terminal domain from the neighboring subunit that forms the roof of the active site (see the inset-i). Substrate binding to the active site on the distal side of the heme induces the organization of a disordered loop, JK-Loop, into a reverse β-turn structure, which sequesters the substrate from the bulk solvent and positions it in a favoring regioorientation for the Trp dioxygenation chemistry.

The indole ring of the substrate Trp occupies the "A" pocket of the active site (see the inset-ii), where it is stabilized by hydrophobic interactions with the surrounding residues (not shown) and an H-bond with H76 on the B-Helix. The carboxylate and ammonium groups extend into the "B" pocket, where they are stabilized by an interlaced H-bonding network with the JK-Loop, the R144 on the D-Helix, and the propionate-7 group of the heme.

IDO and TDO catalyze the same Trp dioxygenation reaction with a similar mechanism,[27] but IDO is a monomer, rather than a tetramer. It contains two domains, the active site domain, which contains a heme, and the N-terminal domain sitting on top of it (Figure S1B). The active site domain shares high structure-based sequence homology with that of TDO. The substrate Trp binds to the distal heme pocket in a binding

Received: June 15, 2024
Revised: July 17, 2024
Accepted: July 23, 2024
Published: August 6, 2024

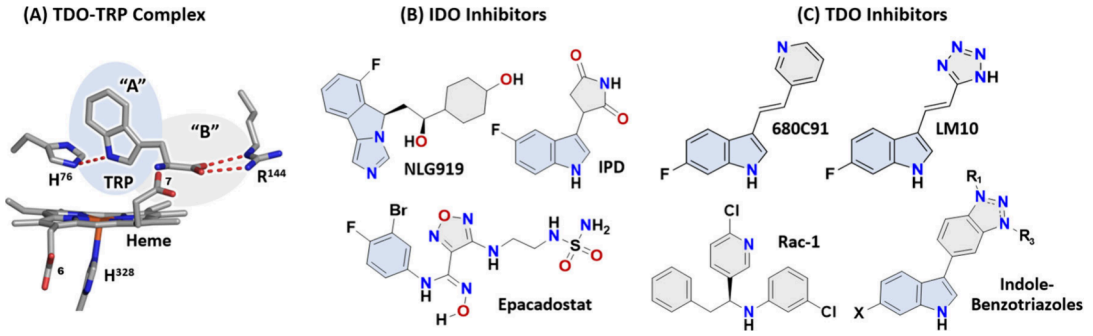

Figure 1. Chemical structures of typical IDO and TDO-selective inhibitors. (A) Active site structure of the TDO-Trp complex (PDB code: 5TIA) highlighting the "A" and "B" pocket of the substrate binding site (in light blue and gray background, respectively). (B–C) Chemical structures of competitive inhibitors targeting the Trp binding sites in IDO and TDO, as well as a new inhibitor, Rac-1, targeting the heme binding site in the apo-form of TDO. The detailed structures of the indole-benzotriazoles studied in this work are illustrated in Table 1.

Table 1. $IC_{50}$and PDB Code Associated with Each TDO Inhibitor Studied in This Work. The IC_{50} Values Were Determined by Spectroscopy-Based Enzyme Assays

Inhibitor	Pharmacophore					IC_{50} (μM)	PDB
NLG919'	Imidazo-isoindole					0.37±0.02	7LU7
LM10	Indole-tetrazole					0.30±0.01	8VZV
Benzotriazole	Indole-Benzotriazoles	Substitution group (R_1 or R_3)		X	Name	IC_{50} (μM)	PDB
	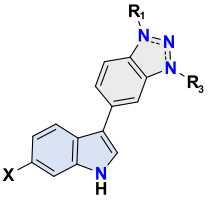	Piperidine 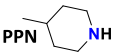	R_3=PPN	H	PPN3	1.65±0.28	8VTQ
			R_1= PPN	H	PPN1	1.01±0.06	8VUG
		Pyrrolidine 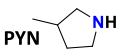	R_3=PYN	H	PYN3	0.69 ± 0.08	8W1H
			R_1=PYN	H	PYN1	1.16 ± 0.04	9B1Q
		Piperazine 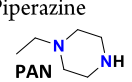	R_3=PAN	H	PAN3	1.26 ± 0.01	9AT2
			R_1=PAN	H	PAN1	0.81 ± 0.02	9B17
			R_3=PAN	F	PAN3F	0.70 ± 0.03	8W2K

pose similar to that in TDO, except that H76 is replaced by S167 that H-bonds with the indoleamine group of the substrate via an intervening water molecule (see the inset-iii).

Despite the similarities in their active site structures, IDO displays several unique structural features distinguishing it from TDO. First, the N-terminal domain present in IDO is absent in TDO, while the Helix–loop–Helix domain present in TDO is absent in IDO. Second, the A-Helix forming the roof of the active site in IDO is from the N-terminal domain, while that in TDO is from the neighboring subunit. Finally, there is a DE-hairpin insertion between the D and E-Helix and an ∼20 residue long extension of the JK-Loop in IDO that are absent in TDO. Despite the differences, the resemblance in the active sites of the two enzymes makes the design of enzyme-selective inhibitors challenging.

A large group of IDO inhibitors with diverse pharmacophores have been developed to date, some of which, such as epacadostat,[28] navoximod (NLG919)[29] and PF-06840003 (IPD)[30] (see Figure 1), have entered clinical trials. Most of these inhibitors are competitive inhibitors, with a large aromatic group occupying the "A" pocket of the Trp binding site and an auxiliary group extending into the "B" pocket. TDO inhibitors, in contrast, are much less developed. Less than a handful of TDO inhibitors have been reported so far, among which 680C91[31] and LM10[15] are two most commonly utilized inhibitors for functional studies of the enzyme. Both inhibitors show an outstanding inhibition potency, with IC_{50} of 0.08 and 0.62 μM, respectively.[11] However, the application of 680C91 is restricted due to its poor solubility and bioavailability,[11] while that of LM10 suffers from instability problems.[20] Recently, two new groups of TDO inhibitors derived from an imidazo-isoindole[32] or indole-tetrazole[20] scaffold, as well as a novel type of inhibitor targeting the heme binding site in the apo-form of the enzyme (Rac-1),[33] have been designed and tested, which show great promise.

To develop enzyme-selective inhibitors, it is essential to comprehend protein-inhibitor interactions at the molecular level. While more than 50 crystal structures of IDO-inhibitor complexes with a wide variety of chemical scaffolds have been documented in the protein data bank, only four structures of TDO in complex with competitive inhibitors that bind to the Trp binding site are available in the protein data bank (PDB codes: 6VBN, 6PYY, 6PYZ and 6A4I). In this work we sought to determine the structures of TDO in complex with a group of competitive inhibitors with three types of pharmacophores: (i) an imidazo-isoindole (NLG919′, a NLG919 analogue where the fluoride and hydroxide on the cyclohexane ring are eliminated), (ii) an indole-tetrazole (LM10), and (iii) seven indole-benzotriazoles (derived from LM10). The structural data offer important new guidelines for the rational design of TDO-selective inhibitors.

https://doi.org/10.1021/acs.jmedchem.4c01360
J. Med. Chem. 2024, 67, 14543–14552

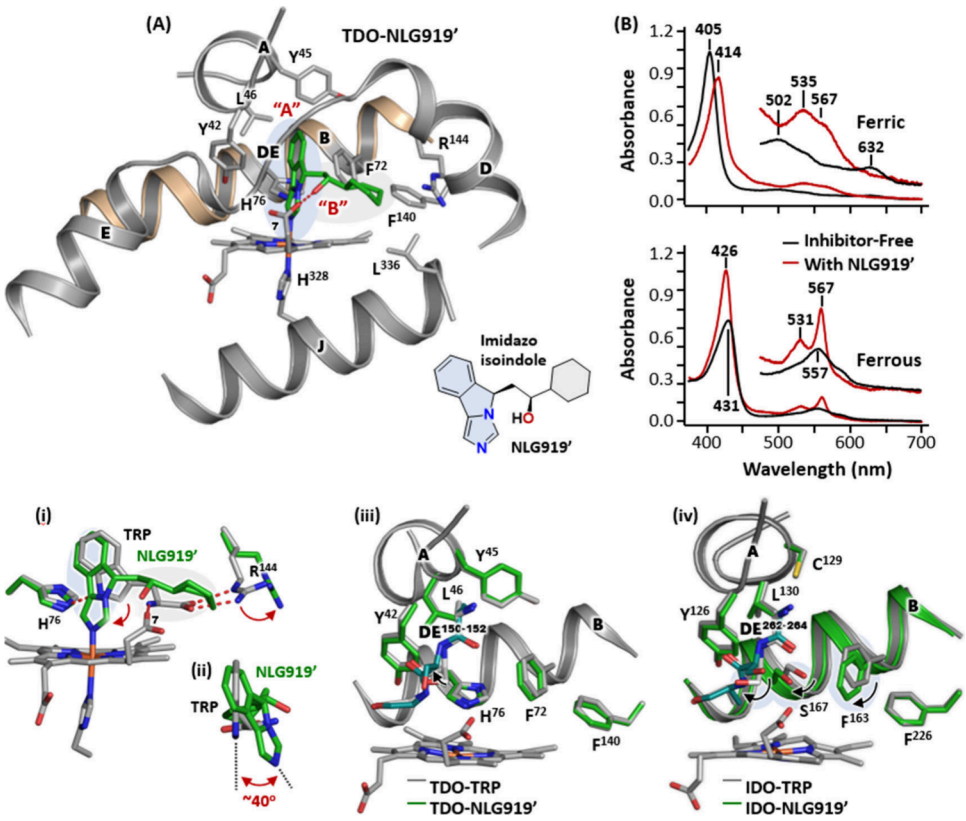

Figure 2. Binding pose of NLG919' in human TDO. (A) The active site structure of the NLG919' complex, with the "A" and "B" pocket highlighted by light blue and gray background, respectively. (B) Absorption spectral changes induced by NLG919' binding to the ferric or ferrous TDO. Insets (i-ii) shows the binding pose of NLG919' superimposed with Trp. The red dotted lines indicate the hydrogen bonds in the Trp complex. Insets (iii-iv) shows the protein conformational changes induced by the substitution of Trp with NLG919' in TDO and IDO, respectively. The inhibitor and substrate are not shown for the sake of clarity. The PDB codes of the TDO-Trp, TDO-NLG919' and IDO-NLG919' complexes are 5TIA, 7LU7 and 5EK3, respectively.

RESULTS AND DISCUSSION

The reported IC_{50} values of the TDO inhibitors studied in this work were measured using either cell- or enzyme-based assays under various pH and temperature conditions and thus are not directly comparable. We first systemically examined the IC_{50} value of each inhibitor using an enzyme-based spectroscopic assay in pH 7.4 Tris buffer, in the presence of 100 μM Trp at 25 °C. The data are shown in Figure S2 and summarized in Table 1. The inhibitory potencies of these inhibitors will be discussed in the context of structure and activity relationships in the ensuing sections.

Crystal Structure of TDO-NLG 919' Complex. NLG919' (Figure 2) is a unique inhibitor as it targets not only IDO (with an IC_{50} of 0.06 μM),[34] but also TDO (with an IC_{50} of 0.37 μM, see Table 1). Here we crystallized TDO in complex with NLG919' and solved its structure with a resolution of 2.30 Å (Table S1). Clear electron density associated with the inhibitor is evident in the active site on top of the heme in each of the four subunits of the tetramer (see an example in Figure S3A). The best modeled structure shows that the imidazo-isoindole group occupies the hydrophobic "A" pocket, formed by the B-Helix, the A-Helix (from the neighboring subunit), the DE-Loop and the heme, where it coordinates to the heme iron via the N atom (Figure 2A). The cyclohexane tail occupies the "B" pocket, flanked by the D-Helix and the DE-Loop, where it extends out into the solvent. The hydroxyl group forms an H-bond with the propionate-7 group of the heme and is within a H-bond distance of the isoindole nitrogen.

Spectroscopic studies show that NLG919' binding to the ferric enzyme induces a shift of the Soret band from 405 to 414 nm and the appearance of two new visible bands at 535/567 nm at the expense of the charge transfer band at 632 nm; while that to the ferrous enzyme leads to a shift of the Soret band from 431 to 426 nm and the conversion of the visible band from 557 to 531/567 nm (Figure 2B). The spectral transitions induced by the NLG919' binding are in good agreement with the coordination of a N-based ligand to the heme iron.[25]

Superimposing the structure of the TDO-NLG919' complex with that of the Trp complex (see the inset-i-ii) reveals that the direct coordination of the inhibitor to the heme iron leads to a ~ 40° tilt of the imidazo-isoindole ring toward the heme iron with respect to the indole ring of the Trp. The conformations of the residues lining the inhibitor binding site, however, remain largely unperturbed upon the substitution of the substrate with the inhibitor (see the inset-iii), except that (i) the DE-Loop (in particular the [150−152] fragment) is slightly pushed out by the bulky imidazo-isoindole ring, (ii) the side chain of R144 (ion-pairing with the carboxylate group of the Trp) swings out into the solvent to accommodate the cyclohexane moiety, and (iii) the JK-Loop (H-bonding with the carboxylate and ammonium groups of the Trp) becomes disordered.

Although the inhibitory potency of NLG919' is ~6-fold lower in TDO with respect to IDO, the binding poses of the inhibitor in the two enzymes are nearly identical (Figure S4). However, the substitution of the substrate Trp with the

https://doi.org/10.1021/acs.jmedchem.4c01360
J. Med. Chem. 2024, 67, 14543−14552

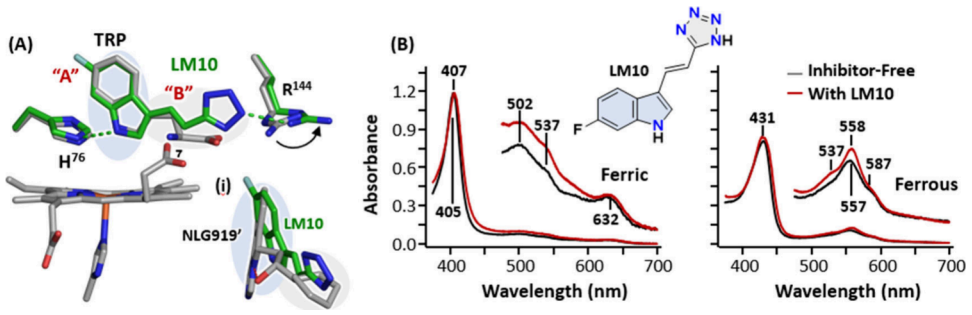

Figure 3. Binding pose of LM10 in human TDO. (A) Superimposed structures of the LM10 and Trp complexes, highlighting their distinct binding poses, and the rotation of the R144 side chain. Inset (i) shows the binding pose of LM10 superimposed with NLG919'. (B) Absorption spectra of ferric or ferrous TDO in the absence or presence of LM10. The PDB codes of Trp and LM10 complexes are 5TIA and 8VZV, respectively.

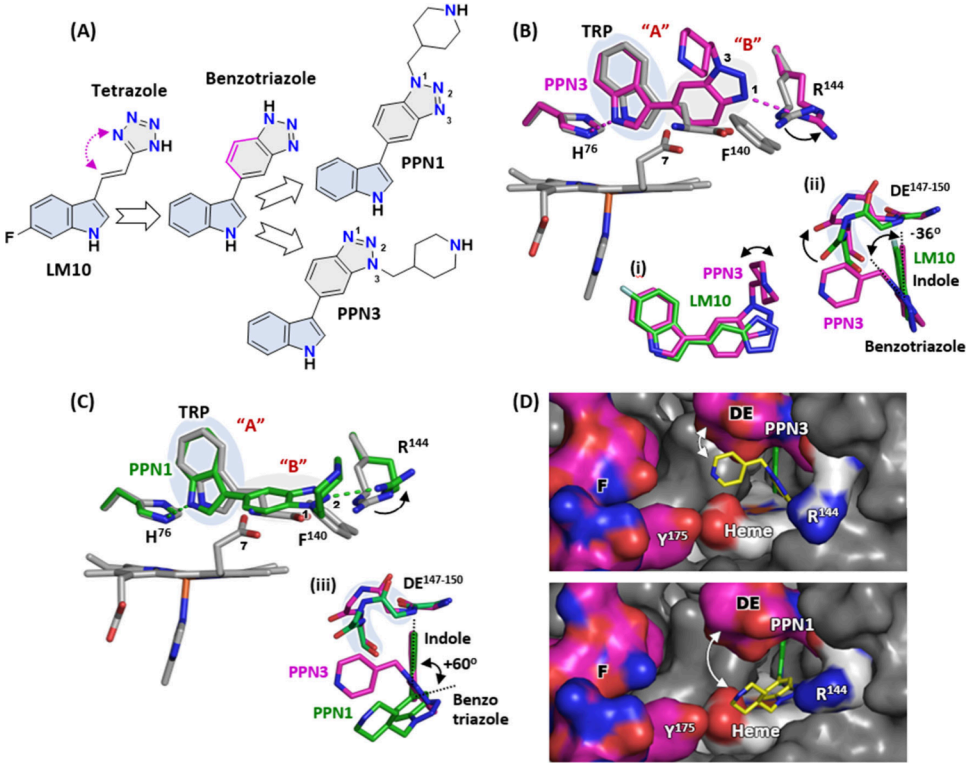

Figure 4. Binding poses of PPN1 and PPN3 in human TDO. (A) Schematic illustration of the design principle of the indole-benzotriazoles using LM10 as the basis. (B–C) Binding poses of PPN3 (green) or PPN1 (magenta) superimposed with Trp bound in the Trp complex (gray). Insets (i-ii) shows the binding pose of PPN3 superimposed with LM10. Inset (iii) shows the binding pose of PPN1 superimposed with PPN3. (D) Surface views of the PPN1 and PPN3 binding sites. The benzotriazole-piperidine group in each complex, highlighted in yellow, is exposed to the bulk solvent. The F-fragment and DE-Loop are colored in magenta. The PDB codes of the Trp, LM10, PPN3 and PPN1 complexes are 5TIA, 8VZV, 8VTQ and 8VUG, respectively.

inhibitor in IDO, unlike that in TDO, leads to significant conformational rearrangement of the active site residues (see the inset-iv). In particular, the side chains of F163 and S167 in the B-Helix forming the base of the inhibitor binding site move forward to interact with the inhibitor; in addition, the DE-Loop undergoes a large-scale rearrangement to accommodate the imidazo-isoindole ring. The structural data suggest that the inhibitor binding site in TDO is rigid, which binds NLG919' in a lock-and-key mode, while that in IDO is more flexible, which binds the inhibitor in an induced-fit mode, allowing the optimization of the protein-inhibitor interactions, thereby accounting for the superior inhibitory potency in IDO versus TDO.

Crystal Structure of TDO-LM10 Complex. We next crystallized TDO in complex with LM10, an indole-tetrazole-based inhibitor that selectively targets TDO. We solved the structure with a resolution of 2.29 Å (Table S1). The overall structure of the complex is similar to that of the NLG919' complex. However, LM10, unlike NLG919', does not coordinate to the heme iron (Figure 3A), which is in good agreement with the spectroscopic data showing that LM10 binding does not perturb the spectral features of the ferric or ferrous enzyme (Figure 3B).

The inhibitor binds to the active site in a trans configuration, with the indole and tetrazole rings occupying the "A" and "B" pocket, respectively, in a nearly coplanar fashion. The fluoride on the indole ring points toward the hydrophobic cavity formed by Y42, Y45 and L46 on the A-Helix (not shown). Superimposing the structure of the LM10 complex with that of the Trp complex shows that the binding pose of the indole ring

https://doi.org/10.1021/acs.jmedchem.4c01360
J. Med. Chem. 2024, 67, 14543−14552

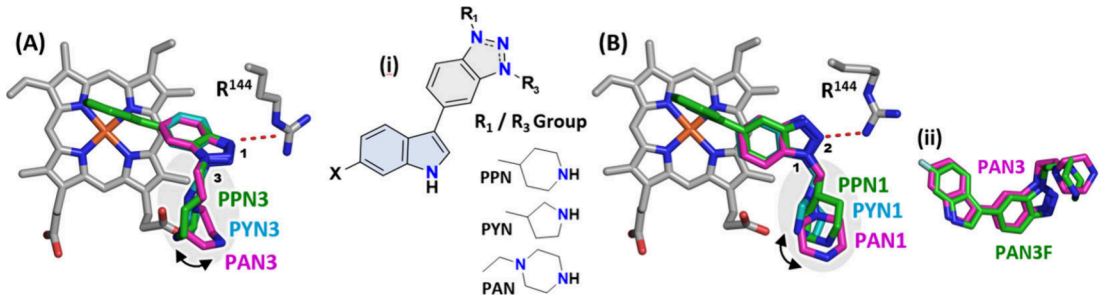

Figure 5. Binding poses of indole-benzotriazole based inhibitors in human TDO. (A,B) Superimposed structures of PPN3/PYN3/PAN3 and PPN1/PYN1/PAN1 complexes, respectively. Inset (i) shows the general structures of the inhibitors. Inset (ii) shows the binding pose of PAN3F superimposed with that of PAN3. The PDB codes of the PPN3/PYN3/PAN3, PPN1/PYN1/PAN1 and PAN3F complexes are 8VTQ/8W1*H*/9AT2, 8VUG/9B1Q/9B17 and 8W2K, respectively.

coincides well with that of Trp, with an H-bond between the indoleamine group and H76. The tetrazole ring forms an additional H-bond with R144, forcing it to lie above the space occupied by the ammonium and carboxyl groups of the substrate in the Trp complex.

The replacement of the substrate Trp with LM10, like that in NLG919′, does not significantly perturb the conformations of the residues forming the binding site (not shown), except that the R144 side chain moves up to interact with the tetrazole ring and that the JK-Loop becomes disordered to accommodate the bulky tetrazole ring. The structure of the LM10 complex, like that of the NLG919' complex, indicates a lock-and-key binding mode. Although the binding poses of LM10 and NLG919' are distinct and neither of them is a snug fit to the binding site, their binding energies are comparable, as indicated by the similar IC_{50} values (0.30 and 0.37 μM, respectively, see Table 1).

Crystal Structures of TDO in Complex with Indole-Benzotriazoles. LM10 has been shown to be valuable for the studies of cellular functions of TDO.[11] However, its clinical application is limited due to the metabolic lability of the vinyl group linking the indole to the tetrazole rings. To overcome this problem, a new group of TDO inhibitors have been developed,[20] where the vinyl and tetrazole ring are fused together by introducing a benzotriazole group (Figure 4A). This new type of inhibitor exhibits much better chemical stability,[20] hence holding great promise as leads in drug development.

To promote the structure-based drug design, we crystallized TDO in complex with three types of indole-benzotriazole based inhibitors, where the N_3 or N_1 of the triazole ring is derivatized with methylpiperidine (PPN3/PPN1), methylpyrrolidine (PYN3/PYN1) or ethylpiperazine (PAN3/PAN1), as well as a fluoride derivative of PAN3 (PAN3F), as listed in Table 1. We determined the structures of these inhibitor complexes with a resolution of 2.05−2.65 Å (Table S1). The overall structures of the inhibitor complexes are analogous to each other and to that of the LM10 complex. Spectroscopic studies show that the binding of the inhibitors to TDO does not perturb its absorption spectra (data not shown), indicating that they, like LM10, do not coordinate to the heme iron, which is in good agreement with the structural data.

In the PPN3 complex (Figure 4B), the indole ring of the inhibitor binds to the "A" pocket of the active site in a binding pose similar to that of Trp, with the indoleamine group forming an H-bond with H76. The benzotriazole moiety occupies the "B" pocket, where it forms an H-bond with R144 via the N_1 atom. Superimposition of the bound PPN3 with LM10 shows that its indole ring overlaps well with that of LM10, while the benzotriazole ring partially overlays with the vinyl-tetrazole group of LM10 (see the inset-i), confirming that the fusion of the two functional groups does not drastically perturb the inhibitor binding pose. The benzotriazole ring rotates −36° away from the indole ring, which causes the piperidine group to swing toward the DE-Loop, pushing the [147−150] fragment away from the heme (see the inset-ii). In the PPN1 complex (Figure 4C), the relocation of the piperidine group from N_3 to N_1 does not perturb the binding pose of the indole ring, but it leads to +60° rotation of benzotriazole ring away from the indole ring (see the inset-iii) and the establishment of a new H-bond between its N_2 atom and the R144 side chain. As such, the piperidine ring, unlike that in the PPN3 complex, does not clash with the DE-Loop.

The binding poses of PYN3/1 and PAN3/1, as well as the conformation of the protein matrix surrounding the inhibitors, resemble those of PPN3/1. The indole rings of the inhibitors coincide well with each other, while the orientation of the benzotriazole rings is dictated by the physical location of the substituent on the ring regardless of its chemical nature (Figure 5), which manifests the importance of the H-bonding interaction with R144. The structure of the PAN3F complex shows that the addition of a fluoride at the C_5 of the indole ring in PAN3 does not significantly perturb the inhibitor binding pose (see the inset-ii), except that the indole ring shifts slightly down toward the heme to accommodate the fluoride.

The inhibitor binding, like that in the LM10 or NLG919' complex, is not a snug fit, as manifested by the ability of the "B" pocket to accommodate the benzotriazole ring in two distinct orientations. The substituent on the benzotriazole ring in the inhibitor complexes extends out into the bulk solvent without direct contact with the protein matrix (Figure 4D). As a result, it exhibits high conformational freedom within the four subunits of a given inhibitor (Figure S5) and significant structural variability among the various inhibitors (Figure 5). This unique structural feature accounts for the fact that the inhibitory potency of the indole-benzotriazoles is not correlated with the physical location or chemical nature of the substituent on the benzotriazole ring (Table 1).

The observation that the IC_{50} values of the indole-benzotriazoles are only slightly higher than that of LM10 (0.30 μM) indicates that the rigidification of the tetrazole ring with respect to the indole ring does not compromise the inhibitory potency. The protein matrices surrounding the indole-benzotriazoles share high structural similarity, manifest-

https://doi.org/10.1021/acs.jmedchem.4c01360
J. Med. Chem. 2024, 67, 14543−14552

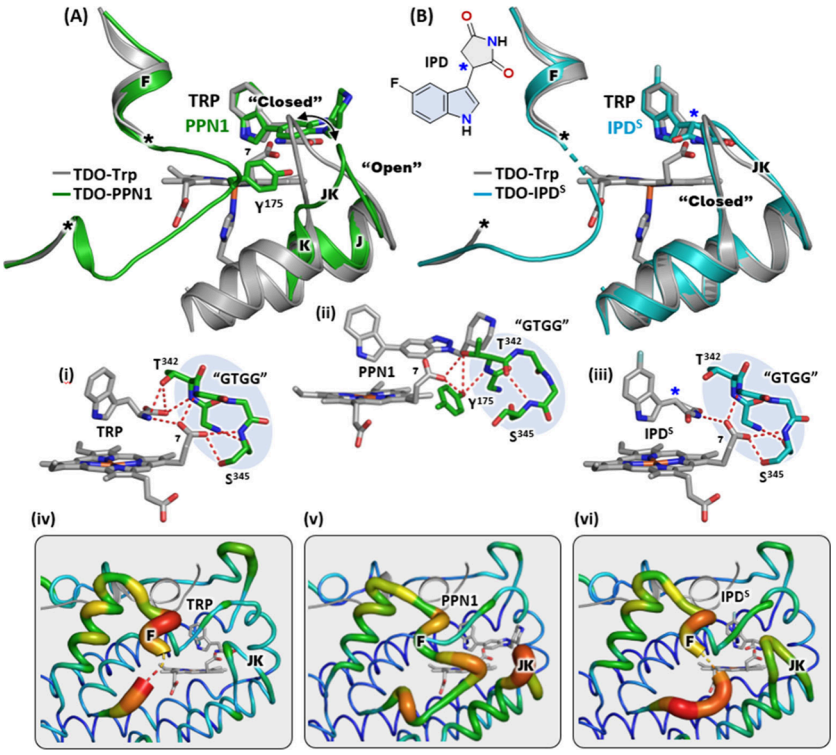

Figure 6. Structural flexibility in the TDO-inhibitor complexes. (A) Superimposed structures of the PPN1 and Trp complexes, highlighting the "open" and "closed" conformations of the JK-Loop. The F-fragment [166−185] in the Trp complex (between the two asterisks) is too flexible to be structurally resolved. (B) Superimposed structures of the IPD^S and Trp complexes, highlighting the "closed" conformations of the JK-Loop. The blue asterisk indicates the chiral center of IPD. Insets (i-iii) show the H-bonding network stabilizing the JK-Loop, in particular the "GTGG" motif and the ensuing S345, in the Trp, PPN1 and IPD^S complexes. Insets (iv-vi) shows the Trp, PPN1, and IPD^S complex structures in the B-factor putty representation, highlighting the distinct conformational freedom of the JK-Loop and F-fragment in each complex. The dashed lines indicate the disordered structural components in the F-fragment. The PDB codes of the Trp, PPN1 and IPD^S complexes are 5TIA, 8VUG and 6PYZ, respectively.

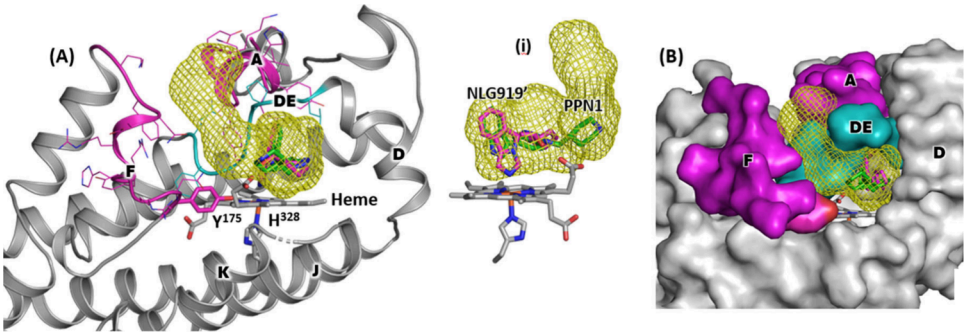

Figure 7. Potential binding pocket for TDO-selective inhibitors. The inhibitor binding pocket (yellow mesh) was generated by the CavitOmiX plugin for PyMOL, using the LM10 complex as the model. The structure of the LM10 complex is shown in cartoon (A) and surface (B) representation (where the bound LM10 is not shown for clarity). The structure is overlaid with NLG919' (magenta) and PPN1 (green). Inset (i) shows the inhibitor binding pocket from a different viewing angle. The dashed line in (A) shows the disordered JK-Loop. The PDB codes of the LM10, PPN1 and NLG919' complexes are 8VZV, 8VUG and 7LU7, respectively.

ing the rigidity of the inhibitor binding site and the lock-and-key binding mode. Nonetheless, the JK-Loop outside the inhibitor binding site exhibits high structural flexibility.

It is well-established that the JK-Loop in the substrate-free enzyme is too flexible to be structurally resolved and that binding of Trp to the active site induces its organization into a reverse β-turn structure (referred to as the "closed" conformation hereinafter, Figure 6A). The "closed" conformer is stabilized by an extended H-bonding network with the carboxylate and ammonium group of the Trp, as well as the propionate-7 group of the heme, via the "GTGG" motif (fully conserved in TDO family of enzymes) and the ensuing S345 residue (see the inset-i).

Similarly, in the structure of TDO in complex with IPD^S, an indole-based inhibitor with a small framework,[35] the JK-Loop adopts the "closed" conformation (Figure 6B). It, however, exhibits significantly higher conformational freedom (see the inset-vi versus inset-iv), plausibly due to the fact that the H-bonding network stabilizing the "closed" conformer is much less extensive (see the inset-iii) as compared to that in the Trp complex. The fact that IPD^S is a weak inhibitor (with IC_{50} of

https://doi.org/10.1021/acs.jmedchem.4c01360
J. Med. Chem. 2024, 67, 14543−14552

424 μM)[35] suggests that the entropy cost for establishing the "closed" conformation is high.

In contrast, in all the inhibitor complex structures examined in this work, the JK-Loop is disordered, due to steric hindrance imposed by the bulky groups occupying the "B" pocket of the inhibitor binding site, except that in the PPN1 complex it assumes a unique "open" conformation (Figure 6A) in two subunits of the tetramer. The "open" conformer is stabilized by the H-bonding network involving Y175 in the F-fragment [166−185] (see the definition in Figure S1) and the propionate-7 group of the heme (see the inset-ii). Its unusually high conformational freedom (see the inset-v) suggests that the JK-Loop in all the inhibitors examined in this work adopts the "open" conformation, some of which are too flexible to be structurally resolved.

The F-fragment, which houses the Y175 residue stabilizing the "open" conformer of the JK-Loop, like the JK-Loop, exhibits high structural flexibility. It is not in direct contact with substances bound in the active site, but the Y175 residue in the F-fragment is critical for controlling product unloading during enzyme turnover, by destabilizing the "closed" conformation of the JK-Loop,[26] suggesting that the outer-sphere interactions between the F-fragment and the JK-Loop may modulate inhibitor affinity.

Using the CavitOmiX plugin for PyMOL, with LM10 complex as a model, we identified an inhibitor binding pocket, extending out of the active site into a valley flanked by the F-fragment and the DE-Loop/A-Helix bundle (Figure 7). This unique binding pocket, which is capable of accommodating all the inhibitors studied in this work (see PPN1 and NLG919' as examples), presents a potential binding target for future drug development.

CONCLUSION

We have systematically examined the binding modes of nine competitive inhibitors with three types of pharmacophores, imidazo-isoindole, indole-tetrazole, and indole-benzotriazole, in TDO. We found that the bound inhibitor in each inhibitor complex is stabilized by hydrophobic interactions with surrounding residues and H-bonding interactions with H76, R144 and/or the propionate-7 group of the heme. The binding pose of each inhibitor is distinct and is not a snug fit, but the inhibitors exhibit similar inhibitory potency, with the IC_{50} values in a narrow window (0.30−1.65 μM). We revealed that the inhibitor binding site in TDO, unlike that in IDO, is rigid, and that the inhibitor binds in a lock-and-key mode. The structural data provide important new insights into structure-based drug design.

EXPERIMENTAL SECTION

Materials. TDO protein was expressed and purified as reported previously.[36,37] NLG919' was purchased from Fisher Scientific ((IDO-IN-7, Cat. No. 502030500, with a purity of 99.93% by LC-MS). LM10 was purchased from Sigma-Aldrich, Inc. (catalog no. SML3499, with a purity of 98% by LC-MS). The indole-benzotriazole based inhibitors were prepared as reported previously.[20] All these compounds are ≥95% pure by HPLC (see Figure S6).

Spectroscopic Measurements. All of the absorption spectra were obtained with a UV2100 spectrophotometer (Shimadzu Scientific Instruments, Inc.) with a spectral slit width of 2 nm. The samples were prepared with 5 μM TDO and 100 μM inhibitor in 50 mM pH 7.4 Tris buffer.

IC_{50} Measurements. The enzyme activity of TDO was determined by the initial linear production rate of the product, N-formyl kynurenine, by measuring the absorbance at 321 nm (ε = 3750 M^{-1} cm^{-1}) as a function of time (within ∼300 s). The reaction was initiated by mixing 100 μM substrate L-Trp and 100 μM ascorbate (as a reductant) with 0.25 μM TDO in 50 mM pH 7.4 Tris buffer containing 150 mM NaCl at 25 °C as reported previously.[36,37] The IC_{50} value of each inhibitor was determined by measuring the enzyme activity as a function of the inhibitor concentration. Each inhibitor stock was prepared in DMSO. The final concentration of DMSO in each assay solution was controlled at 2.0% (v/v).

The relative activity, calculated based on the ratio of the observed activity in the presence versus absence of the inhibitor, was plotted as a function of inhibitor concentration and fitted with the Hill equation described below, where [I] is the inhibitor concentration and n is the Hill coefficient.

$$\text{RelativeActivity} = 1/[1 + (IC_{50}/[I])^{n}] \quad (1)$$

The data summarized in Figure S2 were analyzed with the Origin 8.5 software (OriginLab Corporation).

In addition to the nine inhibitors studied in this work, the IC_{50} value of the lead compound (referred to as BTA) of the indole-benzotriazole group of inhibitors (without R1 and R3 substituents) was measured as a reference. The Hill coefficient n was determined to be ∼1 for all inhibitors except for NLG919' and BTA, which are 1.8 and 3.5, respectively, suggesting significant cooperativity in the inhibitor binding reactions. It is noted that the IC_{50} values reported here for LM10 and the indole-benzotriazoles are in general lower than those reported by Kozlova et al.,[20] which is likely a result of the fundamental differences in the assay methods.

Crystal Preparation. All the TDO crystals were grown using the under-oil microbatch method as reported previously.[26] Briefly, the crystal growth was initiated by mixing a protein solution (45 mg/mL) in 50 mM pH 7.4 Tris buffer, containing 5 mM α-methyl tryptophan and 150 mM NaCl, with a precipitant solution, containing 50 mM sodium citrate, 2% (v/v) Tacsimate and 5% (w/v) PEG 3350 at pH 5.6. Mature TDO crystals were harvested and transferred to the harvest solution containing 100 mM Tris buffer (pH 7.4), 5% (w/v) PEG3350 and 1 mM α-methyl tryptophan. For the NLG919' and LM10 complexes, the harvest solution was the same as the crystallization mother solution. The crystals were reduced with 1 mM sodium dithionite and then washed to remove excess dithionite. They were subsequently soaked with 4 mM inhibitor in 2% (v/v) DMSO for ∼60 min and then cryoprotected by sequentially soaking in 12.5% and 25% (v/v) ethylene glycol for 2 min each before they were flash-frozen in liquid nitrogen for data collection. It is notable that the structures of the TDO-LM10 and TDO-NLG919 complexes can also be obtained with a cocrystallization method and that there is no difference between the structures obtained with the soaking and cocrystallization methods. To be consistent, only the structures with the soaking method are presented here.

Crystallographic Data Collection and Analysis. The crystallographic data were collected by the Lilly Research Laboratories Collaborative Access Team (LRL-CAT) beamline staff at Sector 31 of the Advanced Photon Source or by remote user access at National Synchrotron Light Source II beamline 17-ID-2. The diffraction images were processed through the autoPROC pipeline,[38,39] which were indexed, integrated, and scaled with XDS,[40,41] POINTLESS[42] and AIMLESS.[43] The Karplus-Diederichs method[44] was used to find a proper resolution cutoff for each structure. Molecular replacement was conducted with Phaser[45] through the CCP4i2 graphic interface[46] using the TDO-IPD[S] complex structure (PDB code: 6PYZ) as the search model. Further model building was performed using COOT.[47] Structure refinements were performed using Refmac5.[46,48,49] It is noted that as two of the nine data sets (PDB codes: 9B1Q and 9B17) exhibit significant anisotropy, they were subjected to anisotropic correction by STARANISO.[50] Data processing and refinement statistics are summarized in Table S1. The polder map associated with each inhibitor is shown in Figure S3, based on Subunit D of the tetramer. It should be noted that the electron density maps of each inhibitor in the four subunits of the tetramer are comparable, but Subunit D typically shows the strongest density. The structural

https://doi.org/10.1021/acs.jmedchem.4c01360
J. Med. Chem. 2024, 67, 14543−14552

models were displayed with PyMOL (http://www.pymol.org/). All the structures shown are based on the Subunit D, expect that in Figure 6, which is based on Subunit B, as only the JK-Loop in Subunits A and B displays the "open" conformation.

■ ASSOCIATED CONTENT

Supporting Information

The Supporting Information is available free of charge at https://pubs.acs.org/doi/10.1021/acs.jmedchem.4c01360.

Additional table listing crystallographic data collection and refinement statistics, figures illustrating crystallographic and inhibition data (PDF)

Supply receipt (PDF)

Supply receipt (PDF)

molecular formula strings (CSV)

Accession Codes

PDB codes for the TDO-inhibitor complexes are 7LU7, 8VZV, 8VTQ, 8VUG, 8W1H, 9B1Q, 9AT2, 8W2K, 9B17.

■ AUTHOR INFORMATION

Corresponding Author

Syun-Ru Yeh − *Department of Biochemistry, Albert Einstein College of Medicine, Bronx, New York 10461, United States;* orcid.org/0000-0002-9858-386X; Email: syun-ru.yeh@einsteinmed.edu

Authors

Zachary Geeraerts − *Department of Biochemistry, Albert Einstein College of Medicine, Bronx, New York 10461, United States;* orcid.org/0000-0003-2383-7332

Izumi Ishigami − *Department of Biochemistry, Albert Einstein College of Medicine, Bronx, New York 10461, United States;* orcid.org/0000-0001-6929-1908

Ariel Lewis-Ballester − *Department of Biochemistry, Albert Einstein College of Medicine, Bronx, New York 10461, United States*

Khoa N. Pham − *Department of Biochemistry, Albert Einstein College of Medicine, Bronx, New York 10461, United States*

Arina Kozlova − *Medicinal Chemistry Research Group (CMFA), Louvain Drug Research Institute (LDRI), Université Catholique de Louvain (UCLouvain), Brussels B-1200, Belgium*

Caroline Mathieu − *Medicinal Chemistry Research Group (CMFA), Louvain Drug Research Institute (LDRI), Université Catholique de Louvain (UCLouvain), Brussels B-1200, Belgium*

Raphaël Frédérick − *Medicinal Chemistry Research Group (CMFA), Louvain Drug Research Institute (LDRI), Université Catholique de Louvain (UCLouvain), Brussels B-1200, Belgium;* orcid.org/0000-0001-8119-1272

Complete contact information is available at: https://pubs.acs.org/10.1021/acs.jmedchem.4c01360

Author Contributions

The original draft of this paper was written by S.R.Y. and Z.G.. All authors have given approval to the final version of the manuscript.

Notes

The authors declare no competing financial interest.

■ ACKNOWLEDGMENTS

This work was supported by National Institutes of Health Grants GM151419 and GM115773 to S.-R.Y. and by the Belgian Fonds National de la Recherche Scientifique (F.R.S.-FNRS; Grants 3.05557.43,28252254 and 32704190) and the Fédération Wallonie-Bruxelles (ARC 21/26-115) to R. F.. A.K. and C.M. are PhD fellows of the F.R.S.-FNRS. Seven structures were collected by the Lilly Research Laboratories Collaborative Access Team (LRL-CAT) beamline staff at Sector 31 of the Advanced Photon Source. This research used resources of the Advanced Photon Source, a US Department of Energy (DOE) Office of Science User Facility operated for the DOE Office of Science by Argonne National Laboratory under Contract DEAC02-06CH11357. Use of the Lilly Research Laboratories Collaborative Access Team (LRL-CAT) beamline at Sector 31 of the Advanced Photon Source was provided by Eli Lilly Company, which operates the facility. Two structures were collected at Beamline 17-ID-2 of the National Synchrotron Light Source II, a U.S. Department of Energy (DOE) Office of Science User Facility operated for the DOE Office of Science by Brookhaven National Laboratory under Contract DESC0012704. The authors thank Dr. Denis L. Rousseau for helpful discussions and Séraphin Lacour for his involvement in organic synthesis and fruitful discussions.

■ ABBREVIATIONS

IDO, Indoleamine 2,3-dioxygenase;; IPD, PF-06840003;; NLG919, navoximod;; NLG919', an analog of NLG919;; PAN, ethylpiperazine;; PPN, methylpiperidine;; PYN, methylpyrrolidine;; TDO, Tryptophan dioxygenase;; Trp, L-tryptophan

■ REFERENCES

(1) Lewis-Ballester, A.; Pham, K. N.; Liao, M.; Correia, M. A.; Yeh, S.-R.; Ikeda-Saito, M.; Raven, E. Structure, Function and Regulation of Human Heme-based Dioxygenases. *In Dioxygen-dependent Heme Enzymes* **2018**, 181−221.

(2) Raven, E. L. A short history of heme dioxygenases: rise, fall and rise again. *J. Biol. Inorg. Chem.* **2017**, *22* (2−3), 175−183.

(3) Geng, J.; Liu, A. Heme-dependent dioxygenases in tryptophan oxidation. *Arch. Biochem. Biophys.* **2014**, *544*, 18−26.

(4) Sono, M.; Roach, M. P.; Coulter, E. D.; Dawson, J. H. Heme-Containing Oxygenases. *Chem. Rev.* **1996**, *96* (7), 2841−2888.

(5) Leklem, J. E. Quantitative aspects of tryptophan metabolism in humans and other species: a review. *Am. J. Clin. Nutr.* **1971**, *24* (6), 659−672.

(6) Takikawa, O. Biochemical and medical aspects of the indoleamine 2,3-dioxygenase-initiated L-tryptophan metabolism. *Biochem. Biophys. Res. Commun.* **2005**, *338* (1), 12−19.

(7) Munn, D. H.; Mellor, A. L. Indoleamine 2,3-dioxygenase and tumor-induced tolerance. *J. Clin Invest* **2007**, *117* (5), 1147−1154.

(8) Hou, D. Y.; Muller, A. J.; Sharma, M. D.; DuHadaway, J.; Banerjee, T.; Johnson, M.; Mellor, A. L.; Prendergast, G. C.; Munn, D. H. Inhibition of indoleamine 2,3-dioxygenase in dendritic cells by stereoisomers of 1-methyl-tryptophan correlates with antitumor responses. *Cancer research* **2007**, *67* (2), 792−801.

(9) Friberg, M.; Jennings, R.; Alsarraj, M.; Dessureault, S.; Cantor, A.; Extermann, M.; Mellor, A. L.; Munn, D. H.; Antonia, S. J. Indoleamine 2,3-dioxygenase contributes to tumor cell evasion of T cell-mediated rejection. *Int. J. Cancer* **2002**, *101* (2), 151−155.

(10) Uyttenhove, C.; Pilotte, L.; Theate, I.; Stroobant, V.; Colau, D.; Parmentier, N.; Boon, T.; Van den Eynde, B. J. Evidence for a tumoral immune resistance mechanism based on tryptophan degradation by indoleamine 2,3-dioxygenase. *Nat. Med.* **2003**, *9* (10), 1269−1274.

(11) Pilotte, L.; Larrieu, P.; Stroobant, V.; Colau, D.; Dolusic, E.; Frederick, R.; De Plaen, E.; Uyttenhove, C.; Wouters, J.; Masereel, B.; et al. Reversal of tumoral immune resistance by inhibition of tryptophan 2,3-dioxygenase. *Proc. Natl. Acad. Sci. U. S. A.* **2012**, *109* (7), 2497−2502.
(12) van Baren, N.; Van den Eynde, B. J. Tryptophan-degrading enzymes in tumoral immune resistance. *Front Immunol* **2015**, *6*, 34.
(13) Mullard, A. Immunotherapy interest drives IDO deals. *Nat. Rev. Drug Discovery* **2015**, *14*, 373.
(14) Sheridan, C. IDO inhibitors move center stage in immuno-oncology. *Nat. Biotechnol.* **2015**, *33* (4), 321−322.
(15) Dolusic, E.; Larrieu, P.; Moineaux, L.; Stroobant, V.; Pilotte, L.; Colau, D.; Pochet, L.; Van den Eynde, B.; Masereel, B.; Wouters, J.; et al. Tryptophan 2,3-dioxygenase (TDO) inhibitors. *3-(2-(pyridyl) ethenyl)indoles as potential anticancer immunomodulators. J. Med. Chem.* **2011**, *54* (15), 5320−5334.
(16) Platten, M.; von Knebel Doeberitz, N.; Oezen, I.; Wick, W.; Ochs, K. Cancer Immunotherapy by Targeting IDO1/TDO and Their Downstream Effectors. *Front Immunol* **2015**, *5*, 673.
(17) Austin, C. J.; Rendina, L. M. Targeting key dioxygenases in tryptophan-kynurenine metabolism for immunomodulation and cancer chemotherapy. *Drug Discov Today* **2015**, *20* (5), 609−617.
(18) Winters, M.; DuHadaway, J. B.; Pham, K. N.; Lewis-Ballester, A.; Badir, S.; Wai, J.; Sheikh, E.; Yeh, S. R.; Prendergast, G. C.; Muller, A. J.; et al. Diaryl hydroxylamines as pan or dual inhibitors of indoleamine 2,3-dioxygenase-1, indoleamine 2,3-dioxygenase-2 and tryptophan dioxygenase. *Eur. J. Med. Chem.* **2019**, *162*, 455−464.
(19) Le Naour, J.; Galluzzi, L.; Zitvogel, L.; Kroemer, G.; Vacchelli, E. Trial watch: IDO inhibitors in cancer therapy. *Oncoimmunology* **2020**, *9* (1), 1777625.
(20) Kozlova, A.; Thabault, L.; Liberelle, M.; Klaessens, S.; Prevost, J. R. C.; Mathieu, C.; Pilotte, L.; Stroobant, V.; Van den Eynde, B.; Frederick, R. Rational Design of Original Fused-Cycle Selective Inhibitors of Tryptophan 2,3-Dioxygenase. *J. Med. Chem.* **2021**, *64* (15), 10967−10980.
(21) Platten, M.; Nollen, E. A. A.; Rohrig, U. F.; Fallarino, F.; Opitz, C. A. Tryptophan metabolism as a common therapeutic target in cancer, neurodegeneration and beyond. *Nat. Rev. Drug Discov* **2019**, *18* (5), 379−401.
(22) Coletti, A.; Greco, F. A.; Dolciami, D.; Camaioni, E.; Sardella, R.; Pallotta, M. T.; Volpi, C.; Orabona, C.; Grohmann, U.; Macchiarulo, A. Advances in indoleamine 2,3-dioxygenase 1 medicinal chemistry. *MedChemComm* **2017**, *8* (7), 1378−1392.
(23) Tomek, P.; Palmer, B. D.; Flanagan, J. U.; Sun, C.; Raven, E. L.; Ching, L. M. Discovery and evaluation of inhibitors to the immunosuppressive enzyme indoleamine 2,3-dioxygenase 1 (IDO1): Probing the active site-inhibitor interactions. *Eur. J. Med. Chem.* **2017**, *126*, 983−996.
(24) Sugimoto, H.; Oda, S.; Otsuki, T.; Hino, T.; Yoshida, T.; Shiro, Y. Crystal structure of human indoleamine 2,3-dioxygenase: catalytic mechanism of O2 incorporation by a heme-containing dioxygenase. *Proc. Natl. Acad. Sci. U. S. A.* **2006**, *103* (8), 2611−2616.
(25) Lewis-Ballester, A.; Pham, K. N.; Batabyal, D.; Karkashon, S.; Bonanno, J. B.; Poulos, T. L.; Yeh, S. R. Structural insights into substrate and inhibitor binding sites in human indoleamine 2,3-dioxygenase 1. *Nat. Commun.* **2017**, *8* (1), 1693.
(26) Lewis-Ballester, A.; Forouhar, F.; Kim, S. M.; Lew, S.; Wang, Y.; Karkashon, S.; Seetharaman, J.; Batabyal, D.; Chiang, B. Y.; Hussain, M.; et al. Molecular basis for catalysis and substrate-mediated cellular stabilization of human tryptophan 2,3-dioxygenase. *Sci. Rep* **2016**, *6*, 35169.
(27) Lewis-Ballester, A.; Batabyal, D.; Egawa, T.; Lu, C.; Lin, Y.; Marti, M. A.; Capece, L.; Estrin, D. A.; Yeh, S. R. Evidence for a ferryl intermediate in a heme-based dioxygenase. *Proc. Natl. Acad. Sci. U. S. A.* **2009**, *106* (41), 17371−17376.
(28) Beatty, G. L.; O'Dwyer, P. J.; Clark, J.; Shi, J. G.; Bowman, K. J.; Scherle, P. A.; Newton, R. C.; Schaub, R.; Maleski, J.; Leopold, L.; et al. First-in-Human Phase I Study of the Oral Inhibitor of Indoleamine 2,3-Dioxygenase-1 Epacadostat (INCB024360) in Patients with Advanced Solid Malignancies. *Clin. Cancer Res.* **2017**, *23* (13), 3269−3276.
(29) Nayak-Kapoor, A.; Hao, Z.; Sadek, R.; Dobbins, R.; Marshall, L.; Vahanian, N. N.; Jay Ramsey, W.; Kennedy, E.; Mautino, M. R.; Link, C. J.; et al. Phase Ia study of the indoleamine 2,3-dioxygenase 1 (IDO1) inhibitor navoximod (GDC-0919) in patients with recurrent advanced solid tumors. *J. Immunother Cancer* **2018**, *6* (1), 61.
(30) Crosignani, S.; Bingham, P.; Bottemanne, P.; Cannelle, H.; Cauwenberghs, S.; Cordonnier, M.; Dalvie, D.; Deroose, F.; Feng, J. L.; Gomes, B.; et al. Discovery of a Novel and Selective Indoleamine 2,3-Dioxygenase (IDO-1) Inhibitor 3-(5-Fluoro-1H-indol-3-yl)-pyrrolidine-2,5-dione (EOS200271/PF-06840003) and Its Characterization as a Potential Clinical Candidate. *J. Med. Chem.* **2017**, *60* (23), 9617−9629.
(31) Salter, M.; Hazelwood, R.; Pogson, C. I.; Iyer, R.; Madge, D. J. The effects of a novel and selective inhibitor of tryptophan 2,3-dioxygenase on tryptophan and serotonin metabolism in the rat. *Biochem. Pharmacol.* **1995**, *49* (10), 1435−1442.
(32) Parr, B. T.; Pastor, R.; Sellers, B. D.; Pei, Z.; Jaipuri, F. A.; Castanedo, G. M.; Gazzard, L.; Kumar, S.; Li, X.; Liu, W.; et al. Implementation of the CYP Index for the Design of Selective Tryptophan-2,3-dioxygenase Inhibitors. *ACS Med. Chem. Lett.* **2020**, *11* (4), 541−549.
(33) Lotz-Jenne, C.; Lange, R.; Cren, S.; Bourquin, G.; Goglia, L.; Kimmerlin, T.; Wicki, M.; Müller, M.; Artico, N.; Ackerknecht, S. Discovery and binding mode of a small molecule inhibitor of the apo form of human TDO2. *bioRxiv* **2024**, 574827 DOI: 10.1101/2024.01.09.574827.
(34) Kumar, S.; Waldo, J. P.; Jaipuri, F. A.; Marcinowicz, A.; Van Allen, C.; Adams, J.; Kesharwani, T.; Zhang, X.; Metz, R.; Oh, A. J.; et al. Discovery of Clinical Candidate (1R,4r)-4-((R)-2-((S)-6-Fluoro-5H-imidazo[5,1-a]isoindol-5-yl)-1-hydroxyethyl)cyclohexan-1-ol (Navoximod), a Potent and Selective Inhibitor of Indoleamine 2,3-Dioxygenase 1. *J. Med. Chem.* **2019**, *62* (14), 6705−6733.
(35) Pham, K. N.; Lewis-Ballester, A.; Yeh, S. R. Structural Basis of Inhibitor Selectivity in Human Indoleamine 2,3-Dioxygenase 1 and Tryptophan Dioxygenase. *J. Am. Chem. Soc.* **2019**, *141* (47), 18771−18779.
(36) Batabyal, D.; Yeh, S. R. Substrate-protein interaction in human tryptophan dioxygenase: the critical role of H76. *J. Am. Chem. Soc.* **2009**, *131* (9), 3260−3270.
(37) Batabyal, D.; Yeh, S. R. Human tryptophan dioxygenase: a comparison to indoleamine 2,3-dioxygenase. *J. Am. Chem. Soc.* **2007**, *129* (50), 15690−15701.
(38) Vonrhein, C.; Flensburg, C.; Keller, P.; Sharff, A.; Smart, O.; Paciorek, W.; Womack, T.; Bricogne, G. Data processing and analysis with the autoPROC toolbox. *Acta Crystallogr. D Biol. Crystallogr.* **2011**, *67*, 293−302.
(39) Vonrhein, C.; Flensburg, C.; Keller, P.; Fogh, R.; Sharff, A.; Tickle, I. J.; Bricogne, G. Advanced exploitation of unmerged reflection data during processing and refinement with autoPROC and BUSTER. *Acta Crystallogr. D Struct Biol.* **2024**, *80*, 148−158.
(40) Otwinowski, Z.; Minor, W. Processing of X-ray diffraction data collected in oscillation mode. *Method Enzymol* **1997**, *276*, 307−326.
(41) Kabsch, W. *Acta Crystallogr. D Biol. Crystallogr.* **2010**, *66*, 125−132.
(42) Evans, P. Scaling and assessment of data quality. *Acta Crystallogr. D Biol. Crystallogr.* **2006**, *62*, 72−82.
(43) Evans, P. R.; Murshudov, G. N. How good are my data and what is the resolution? *Acta Crystallographica Section D* **2013**, *69* (7), 1204−1214.
(44) Karplus, P. A.; Diederichs, K. Linking crystallographic model and data quality. *Science* **2012**, *336* (6084), 1030−1033.
(45) McCoy, A. J.; Grosse-Kunstleve, R. W.; Adams, P. D.; Winn, M. D.; Storoni, L. C.; Read, R. J. Phaser crystallographic software. *J. Appl. Crystallogr.* **2007**, *40*, 658−674.
(46) Winn, M. D.; Ballard, C. C.; Cowtan, K. D.; Dodson, E. J.; Emsley, P.; Evans, P. R.; Keegan, R. M.; Krissinel, E. B.; Leslie, A. G. W.; McCoy, A.; McNicholas, S. J.; Murshudov, G. N.; Pannu, N. S.;

Potterton, E. A.; Powell, H. R.; Read, R. J.; Vagin, A.; Wilson, K. S. Overview of the CCP4 suite and current developments. *Acta Crystallogr. D Biol. Crystallogr.* **2011**, *67*, 235−242.
(47) Emsley, P.; Cowtan, K. Coot: model-building tools for molecular graphics. *Acta Crystallogr. D Biol. Crystallogr.* **2004**, *60*, 2126−2132.
(48) Murshudov, G. N.; Skubak, P.; Lebedev, A. A.; Pannu, N. S.; Steiner, R. A.; Nicholls, R. A.; Winn, M. D.; Long, F.; Vagin, A. A. REFMAC5 for the refinement of macromolecular crystal structures. *Acta Crystallogr. D Biol. Crystallogr.* **2011**, *67*, 355−367.
(49) Murshudov, G. N.; Vagin, A. A.; Dodson, E. J. Refinement of macromolecular structures by the maximum-likelihood method. *Acta Crystallogr. D Biol. Crystallogr.* **1997**, *53*, 240−255.
(50) Tickle, I. J.; Flensburg, C.; Keller, P.; Paciorek, W.; Sharff, A.; Vonrhein, C.; Bricogne, G. *STARANISO*. Global Phasing Ltd., Cambridge, United Kingdom, 2016. http://staraniso.globalphasing.org/cgi-bin/staraniso.cgi (accessed June 6, 2024).

https://doi.org/10.1021/acs.jmedchem.4c01360
J. Med. Chem. 2024, 67, 14543−14552